processes

MDPI

Article

Investigation of the Cold Working Effect on the Corrosion Resistance of 1.4301 Stainless Steel

Péter Pató [1], Ferenc Haraszti [2], Zoltán Nyikes [3,*] and Tünde Anna Kovács [2,*]

[1] Doctoral School on Safety and Security Sciences, Obuda University, 1081 Budapest, Hungary
[2] Bánki Donát Faculty of Mechanical and Safety Engineering, Obuda University, 1081 Budapest, Hungary
[3] Milton Friedman University, 1039 Budapest, Hungary
* Correspondence: nyikes.zoltan@bgk.uni-obuda.hu (Z.N.); kovacs.tunde@bgk.uni-obuda.hu (T.A.K.)

Abstract

This research investigated the effect of cold working on the corrosion resistance of 1.4301 (X5CrNi18-10, AISI 304) austenitic stainless steel. The test specimens were prepared by cold rolling. The original thickness of the austenitic steel was 3.0 mm. Cold rolling produced specimens with thicknesses of 2.5, 2.0, 1.5, 1.0, and 0.65 mm. A corrosion test was conducted according to ASTM G48 in a 6% ferric chloride solution for 45 h. The corrosion process caused weight loss, which was measured for all test specimens. The corrosion test results showed a clear correlation between deformation and corrosion-induced weight loss. Corrosion weight loss depended on the degree of cold working. Based on these results, the PREN index—which can be determined from the chemical composition—is not sufficient on its own to characterise the corrosion resistance of 1.4301 austenitic stainless steel, as the degree of cold working significantly modifies the extent of corrosion resistance.

Keywords: stainless steel; corrosion; pitting corrosion; PREN

1. Introduction

The corrosion resistance of stainless steel is due to a thin passive layer that forms in an oxidising environment on the surface. Chromium plays a decisive role in the formation of this passive layer as Cr_2O_3 [1]. The layer consists mainly of chromium oxides, and it significantly reduces the rate of electrochemical reactions between the metal and its environment [2]. Under appropriate conditions, the passive layer can reform following local damage; therefore, the corrosion behaviour of stainless steels differs significantly from that of ordinary carbon and alloy steels. However, corrosion resistance is not an absolute property: the corrosion behaviour of a given steel is determined jointly by its alloy composition and the corrosive environment [3,4]. Passive-film characterisation by XPS and electrochemical methods has also revealed the relevance of film chemistry and electronic properties to stainless-steel passivity [5–7]. A general mechanistic overview separates passivity breakdown, metastable pit formation and pit propagation [8].

In the case of stainless steels, therefore, corrosion damage often does not take the form of uniform material loss, but rather as a localised corrosion process. Pitting corrosion, which occurs in media containing chloride ions, is particularly significant. Chloride ions can promote the localised destabilisation of the passive layer, resulting in the formation of a small active area. This area behaves as an anode relative to the surrounding surface, which remains passive, thus significantly increasing the density of the localised corrosion current [9]. In the developing corrosion cavity, the pH decreases due to the hydrolysis of

Check for updates

Academic Editor: Haibin Zuo

Received: 9 October 2026
Revised: 29 October 2026
Accepted: 3 November 2026
Published: 5 November 2026

Copyright: © 2026 by the authors. Licensee MDPI, Basel, Switzerland. This article is an open access article distributed under the terms and conditions of the Creative Commons Attribution (CC BY) license.

metal ions, while the concentration of chloride ions may increase, causing the corrosion environment inside the cavity to become increasingly aggressive. If the process becomes self-sustaining, the initially small hole can rapidly deepen [1,3,4,10]. Early work on pit initiation established the particular significance of sulphide particles and their dissolution products, while later local chemical mapping refined the proposed mechanisms [11–13]. Highly purified 1.4301 alloys provide an additional means of isolating non-metallic inclusion effects [14]. Metastable pitting, as quantified by short-lived current transients, should be differentiated from sustained pit growth [15].

In addition to alloy composition, the formation and propagation of pitting corrosion are also influenced by metallurgical and surface characteristics. In addition to chromium, molybdenum and nitrogen play a particularly important role in increasing resistance to pitting and crevice corrosion [1,2,16]. At the same time, corrosion behaviour can also be modified by the microstructure, the presence of secondary phases, and non-metallic inclusions [17,18]. Studies of oxide particles, inclusion engineering and sulphide-free alloy conditions indicate that inclusion chemistry, morphology and processing history can affect the probability of local attack [19–21]. More recent work on cerium-modified inclusions supports an inclusion-sensitive interpretation of pit initiation in 1.4301 stainless steel [22]. Reviews of inclusion formation in stainless steel production further demonstrate why alloy specifications do not uniquely determine inclusion populations [23].

Both electrochemical and accelerated immersion methods can be used to test the corrosion properties of stainless steels. The advantage of immersion testing is that test specimens can be exposed to a controlled, aggressive corrosive medium for a specified period of time, after which the corrosion damage can be characterised by weight loss and morphological examination of the surface [18]. The purpose of corrosion testing may be, on the one hand, to elucidate the mechanism of a corrosion process and, on the other hand, to compare the resistance of different materials or material states in a given environment [2,10,24]. The ASTM G48 ferric-chloride immersion procedure provides a comparative test protocol, whereas cleaning and mass-loss evaluation need to be considered separately under ASTM G1 [25,26]. Electrochemical corrosion testing has also been reviewed in the related field of biomedical titanium alloys; such methods provide methodological context but cannot substitute for direct 1.4301-steel evidence [27].

The Pitting Resistance Equivalent Number (PREN) is an indicator widely used to preliminarily characterise the resistance of stainless steels to localised corrosion [1–3]. PREN is a dimensionless value calculated from the chemical composition of the alloy, which is primarily used to compare the expected resistance to pitting corrosion of different stainless steel grades [1,2,24,28]. The most commonly used formula takes into account the chromium, molybdenum, and nitrogen content, calculated by the following Equation (1): The composition-based indicator is helpful for alloy screening, but its interpretation requires care when comparing specimens of the same grade after different processing histories [29].

$$\mathrm{PREN} = \%\mathrm{Cr} + 3.3 \times \%\mathrm{Mo} + 16 \times \%\mathrm{N}, \quad (1)$$

where Cr, Mo, and N represent the chromium, molybdenum, and nitrogen content of the alloy, expressed as a percentage by weight. For certain stainless steels—primarily those with higher alloy content—PREN relationships that also take into account additional alloying elements, such as tungsten, are used [1,30,31]. Studies of nitrogen-containing, cold-worked austenitic steels have reported responses that vary with both the alloying level and deformation range [32].

An increase in PREN generally indicates greater theoretical pitting corrosion resistance; therefore, this value is suitable for a quick, composition-based comparison of the corrosion resistance of different steel grades [33]. Its use is particularly useful in the initial stages

of material selection; however, PREN cannot be considered a comprehensive indicator of actual corrosion behaviour. Even among steels with identical or similar PREN values, there may be significant differences in actual pitting corrosion resistance, since the calculation takes into account only specific elements of the chemical composition. Furthermore, actual corrosion behaviour can also be influenced by microstructure, inclusions, surface quality, heat treatment, and environmental effects. For this reason, the literature emphasises that the calculated PREN value should primarily be used for a rough comparison of different steel grades, and that it cannot, on its own, be used to draw comprehensive conclusions about the expected corrosion behaviour in a given operating environment [1,34,35]. Cold rolling has been examined directly in 1.4301 (AISI 304) using electrochemical techniques, and non-monotonic changes in pitting resistance have also been observed under conditions different from the present ferric-chloride exposure [36,37]. Residual strain, crystal defects and post-rolling thermal treatment have likewise been shown to influence the surface response of stainless steel [38].

When determining the corrosion behaviour of stainless steels, experimental tests are therefore necessary in addition to indicators based on chemical composition [39]. The ferric chloride (iron(III)-chloride, $FeCl_3$) immersion test is particularly suitable for comparing the resistance of stainless steels to localised corrosion, primarily pitting and crevice corrosion. During such tests, the aggressive, chloride-ion-rich medium accelerates the local failure of the passive layer, allowing for a comparison of the corrosion behaviour of different material conditions over a short period of time. Depending on the nature of the corrosion damage, the test results can be evaluated based on weight loss, microscopic examination of the corroded surface, or electrochemical and other quantitative characteristics. However, weight loss primarily characterises overall material loss; therefore, in cases of localised corrosion, surface morphological examination serves as an important supplement to it [40]. For the interpretation of immersion-induced mass loss, it should therefore be recognised that corrosion current, pit initiation density, pit depth and total material removal represent different aspects of degradation [15].

Based on the findings in the literature, the corrosion behaviour of stainless steels is therefore the result of several interacting factors. The PREN, calculated based on chemical composition, is an important and widely used comparative parameter for estimating pitting corrosion resistance; however, evaluating actual corrosion behaviour also requires controlled experimental tests and consideration of the material's state characteristics. This is also supported by research indicating that microstructure, inclusions, and the condition of previous plastic deformation can measurably influence passivation and the development of localised corrosion [24,41]. The objective of this study is to investigate, using immersion testing, the corrosion susceptibility of 1.4301 stainless steel as a function of the degree of plastic deformation. Evidence from mechanically deformed austenitic steels has highlighted the combined contributions of grain refinement, deformation rate, dislocation density and strain-induced martensite [42–44]. Cold working induces residual stresses in the austenitic steel structure, which reduce corrosion resistance [36,45]. The microstructural reasons for corrosion in cold-worked stainless steels are as follows: (1) grain boundaries, (2) second phases or precipitates, (3) inclusions and impurities, (4) dislocations and residual stresses, (5) phase differences [46,47].

(1) In the grain boundaries, the energy is higher, the disorder is greater, and the chemical reactivity is higher than within the grains. This explains selective damage, such as intergranular corrosion [48].
(2) Second phases or precipitates embedded in the metal have a different composition and electrode potential than the surrounding matrix. This potential difference creates a micro-galvanic cell [49].

(3) Non-metallic inclusions—such as manganese sulfides (MnS) in steel—act as breakdown sites for protective surface oxides, frequently triggering pitting corrosion [50].
(4) Deformation increases dislocation density, which decreases corrosion resistance. In the case of the barrier in the slip plane, the accumulation of dislocations is generally interpreted as a mechanism for increasing hardness, which results in a significant increase in the deformation energy per dislocation [46]. Areas with high dislocation densities store excess mechanical strain energy from cold working. Higher internal energy increases the thermodynamic drive for localised dissolution and stress-corrosion cracking [51,52].
(5) Plastic deformation induces phase transformation in austenitic steels. Martensitic transformation induced by plastic deformation occurs when, under the influence of mechanical work or stress, a metastable crystal structure—most commonly austenite (face-centred cubic, FCC) in stainless steels—transforms into a martensitic phase (such as hexagonal close-packed ε-martensite or body-centred cubic/tetragonal α'-martensite) without diffusion [53].

In cases where multiple phases appear in the microstructure, galvanic corrosion also occurs. All effects that cause structural inhomogeneity can reduce corrosion resistance. In stainless steels, low dislocation density, low residual stress, and a uniform microstructure are desired to ensure corrosion resistance [45,54].

2. Material and Method

2.1. The Used 1.4301 Stainless Steel

In the tests, we used an austenitic stainless steel with the material number EN 1.4301 (EN 10088-3) X5CrNi18-10 or AISI 304 (ASTM A240/ASME SA240) stainless steel, which is characterised by good corrosion resistance as well as favourable formability and weldability. Grade 1.4301 belongs to the class of Cr–Ni austenitic stainless steels. The standard chemical composition of Steel Grade 1.4301 is shown in Table 1. Prior studies on AISI 304 link increasing cold reduction with work hardening and changes in the phase balance; these observations provide a reference for interpreting the hardness measurements below [45,54].

Table 1. Standard chemical composition of Steel Grade 1.4301.

Material	C	Cr	Ni	Si	Mn	P	S	Mo
wt (%)	≤0.07	17.5–19.5	8–10.5	≤1.00	≤2.00	≤0.045	≤0.045	-

In the case of 1.4301, the molybdenum and nitrogen content is low, so the PREN value is primarily determined by the chromium content. Taking into account the standard chemical composition range, the PREN value typical for 1.4301 is within the range of 17.5–21.1.

2.2. Preparation of Test Specimens

The original test material consisted of laser-cut sheets with a thickness of 3 mm, nominal dimensions of 5 × 200 mm, and material grade 1.4301. We cold-rolled the cut sheets in stages, with nominal thickness reductions of 0.5 mm per step. During rolling, we produced six different sheet thicknesses: 3.0, 2.5, 2.0, 1.5, 1.0, and 0.65 mm. Comparable rolled 1.4301 steel specimens have been investigated in studies addressing the interaction of forming history with localised corrosion, including welded material [55].

We prepared test specimens from each rolling condition for the corrosion test. We selected the test specimen dimensions so that, for each sheet thickness, the surface area in contact with the corrosive medium was nearly identical. This is essential for the corrosion

test, as differences in initial surface area alone could influence weight loss. Using the same surface area allows a more direct comparison of the corrosion behaviour of material conditions cold-rolled to varying degrees.

The test specimens thus represented six different rolling conditions, with varying degrees of plastic deformation relative to the initial sheet thickness of 3.0 mm. In subsequent tests, we prepared these specimens according to the specified procedures and measured weight loss after the corrosion test.

To ensure unambiguous identification, the test specimens were labelled with a letter and a serial number. The letter indicated the sheet thickness corresponding to the given test specimen, while the serial number identified each test specimen from the same sheet thickness individually (Table 2).

Table 2. Thickness of the tested specimens.

Thickness (mm)	3	2.5	2	1.5	1	0.65
Designation	A1, A2, A3	B1, B2, B3	C1, C2, C3	D1, D2, D3	E1, E2, E3	F1, F2, F3

Accordingly, we included a total of 18 test specimens in the corrosion test. We engraved unique identifiers on the test specimens to ensure they could be identified after immersion in the corrosive medium.

2.3. Hardness and Surface Roughness Measurement

The mechanical properties of the material under investigation are influenced by both the starting material condition and the degree of subsequent cold rolling. In austenitic stainless steels, cold forming can cause significant work hardening, accompanied by increased strength. Therefore, we also determined the hardness of test specimens rolled to varying degrees. We performed the hardness tests using a Buehler Wilson UH4750 universal digital hardness tester (Buehler, Lake Bluff, IL, USA). Table 3 below shows the average hardness values as a function of sheet thickness. We used the Vickers method with a 0.2 kg indenter (HV 0.2) to determine hardness. We took three measurements for each sheet thickness, and the table summarises the average hardness values. The increase in hardness should be interpreted in conjunction with possible changes in dislocation density and transformation-induced martensite rather than being attributed to phase transformation alone [56].

Table 3. Average hardness values as a function of sheet thickness.

Thickness (mm)	3	2.5	2	1.5	1	0.65
Hardness (HV 0.2)	183.4	320.77	341.47	411.96	436.26	494.61

To characterise the test specimens' surface condition, we also measured surface roughness using a Mitutoyo Surftest SJ-301 universal surface roughness tester (Mitutoyo, Kawasaki-shi, Japan). Surface roughness varied within a fairly narrow range; the average roughness (Ra) for each sheet thickness ranged from 0.353 to 0.457 µm. The lowest average Ra value was measured for the 2 mm-thick sheets, while the highest was measured for the 3-mm-thick sheets. The roughness values did not change monotonically with the degree of rolling; no significant differences in surface roughness were observed among the various rolling conditions. Therefore, when evaluating the corrosion tests, this parameter is presumably less important than the effect of rolling. Table 4 below shows the average surface

roughness values, which vary by sheet thickness. We took three measurements on two test specimens for each sheet thickness, for a total of six measurements per thickness; the table presents their average.

Table 4. Average surface roughness values (Ra).

Thickness (mm)	3	2.5	2	1.5	1	0.65
Ra (µm)	0.457	0.414	0.353	0.398	0.374	0.435

2.4. Parameters of the ASTM G48 Corrosion Test

The corrosion test was conducted in accordance with the principles of the ferric chloride pitting corrosion test specified in Method A of the ASTM G48 standard. The ASTM G48 standard evaluates the resistance of stainless steels and other alloys to pitting and crevice corrosion in an oxidising chloride medium. The test medium for Method A is a ferric chloride solution of approximately 6% by weight, for which the standard also recommends a test temperature of 22 ± 2 °C. The specified solution, duration and temperature should be reported explicitly because accelerated ferric-chloride results are condition-dependent and cannot be equated directly with general service-life performance [25]. Surface damage under repeated particle impingement has separately been examined in erosion–corrosion studies; those loading conditions should not be conflated with static immersion [57].

During the test, the test specimens were individually immersed in 20 mL of a 6% (by weight) ferric chloride solution at 22.5 °C for 45 h. We cleaned the test specimen surfaces with acetone before the test and, after the corrosion test, cleaned them with distilled water and acetone to remove corrosion products and contaminants. We tested three specimens at each plate thickness. Specimen cleaning and the possible influence of residual deposits on measured mass loss are also recognised methodological considerations [26].

We determined the corrosion test results based on the difference in weight of the test specimens before and after immersion in the corrosive medium. We compared the corrosion behaviour under the various rolling conditions based on weight loss. To measure weight loss, we used a Kern ALJ 220-4NM analytical balance (KERN & Sohn GmbH, Balingen-Frommern, Germany).

2.5. Preparation for Microscopy Test

To examine the microstructure of test specimens with different plate thicknesses and varying degrees of cold rolling, we prepared microscopic images of the microstructure for each rolling condition. For metallographic examination, we cold-embedded the test specimens; after grinding and polishing, we etched the surfaces with Kalling's etchant. To prepare the microscopic images, we used an Olympus DSX1000 opto-digital measuring microscope (Olympus, Tokyo, Japan) and captured images at 2400× magnification.

3. Results and Discussion

3.1. Results of the Microscopic Examination

The microscopic images clearly show the gradual formation of work-hardening martensite as sheet thickness decreases, i.e., as the degree of cold forming increases (see Figure 1). The microstructures corresponding to the various rolling conditions thus clearly illustrate the microstructural changes resulting from cold rolling. In the case of the most heavily formed test specimens with the thinnest sheet thickness, the presence of work-hardening martensite is more pronounced than in test specimens subjected to a lower degree of cold forming. Microscopy showed that the martensitic needle structure varies with the degree

of forming (Figure 1). The reference specimen (3 mm thickness) microstructure is uniform austenite. It shows typical twin crystals and polygonal grain geometry. In microscopic images of the formed test specimens, martensite appears as a needle-like phase that remains darker along the forming bands or at their intersections. The microscopic image of the 2.5 mm-thick test specimen shows the onset of martensitic transformation, while the boundaries of the original austenitic grains are still partially preserved. Subsequent microscopic images show that as the degree of work hardening increases, the original grain boundaries disappear and the martensite needles become finer. The martensite fraction in the microstructure increases. Deformation-induced martensite in 1.4301 stainless steel has been documented using direct observations and related electrochemical measurements; phase quantification would nevertheless require an appropriate independent measurement [58].

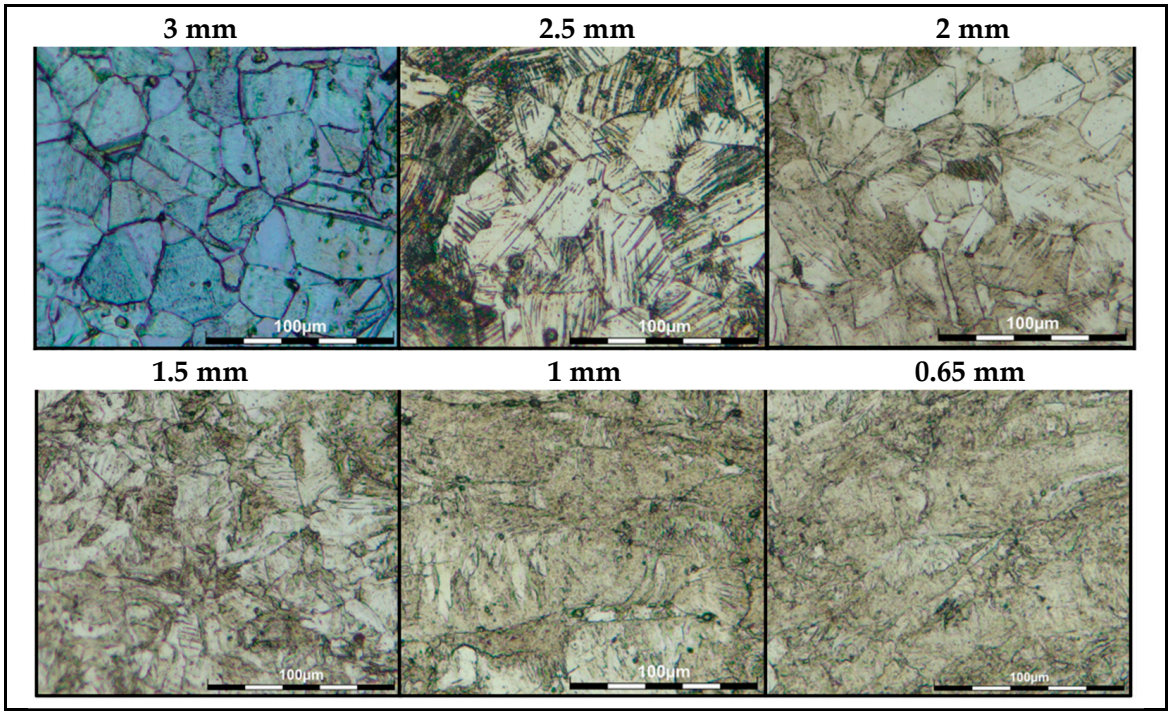


Figure 1. Microscopic images of the test specimens.

3.2. Results of the Corrosion Test

Figure 2 below shows the average weight losses of the test specimens during the corrosion test, by forming degree (sheet thickness). Based on the results, it is clearly evident that as the sheet thickness decreases—that is, as the degree of forming during cold rolling increases—the weight loss of the test specimens gradually increases. The smallest weight loss was measured for the test specimens in their initial, unformed state with a thickness of 3.0 mm, while the largest weight loss values were obtained for the test specimens with a thickness of 0.65 mm, which were formed to the greatest extent. This trend is consistent with experimental findings on some cold-deformed steels, although the magnitude and even direction of the effect depend on the strain range, environment, residual stresses, and alloy state [56,57].

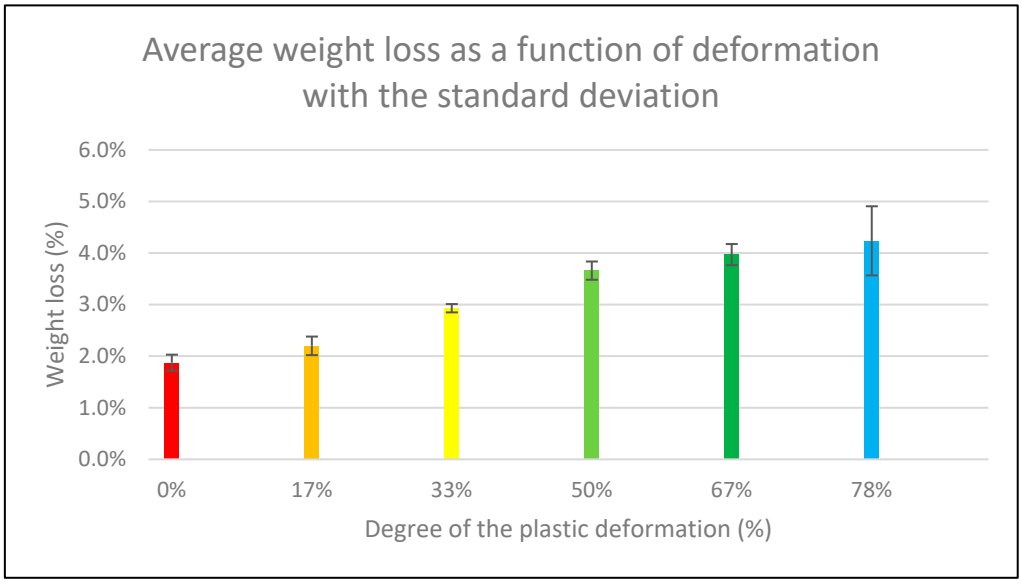


Figure 2. Average weight loss as a function of deformation.

Based on a comparison of the weight losses associated with the different rolling conditions, a clear correlation can therefore be observed between the degree of forming and the weight loss occurring during the corrosion test. The increase in weight loss suggests that as the degree of cold forming increased, the tested material's corrosion behaviour became less favourable. Figure 2 also illustrates the table results and clearly shows the relationship between weight loss and the degree of plastic deformation. For example, tensile deformation, immersion media, and rolling history have produced different responses in classic and contemporary studies; this prevents inferring a universal monotonic rule from the present dataset [32,36,37].

The results show that corrosion-induced material loss increases due to microstructural changes. The number of dislocations can increase as a result of the forming process, and martensite appears in increasing quantities in the microstructure. As a result of the forming process, residual stress in the test specimen can increase. Microstructural changes during cold forming, as a function of the degree of plastic deformation, caused the increase in corrosion weight loss (Figure 2). Based on the results, we cannot establish an equation relating corrosion weight loss to the degree of plastic deformation during cold forming, but the relationship is clear.

3.3. Macroscopic Examination of the Corroded Surface

After the corrosion test, we also took macroscopic images of the test specimen surfaces exposed to corrosion using an Olympus DSX1000 opto-digital measuring microscope (see Figure 3). The images clearly show corrosion lesions and, in some places, localised surface pitting; however, as the sheet thickness decreases—that is, as the degree of forming increases—the number of visible pits or pitting lesions shows no clear or monotonic change. Macroscopic images are therefore not suitable on their own for a clear quantitative comparison of corrosion extent. Surface imaging is valuable for identifying individual pits; however, the lack of a monotonic trend in visible pit counts should not be interpreted as no change in mass loss [8,15].

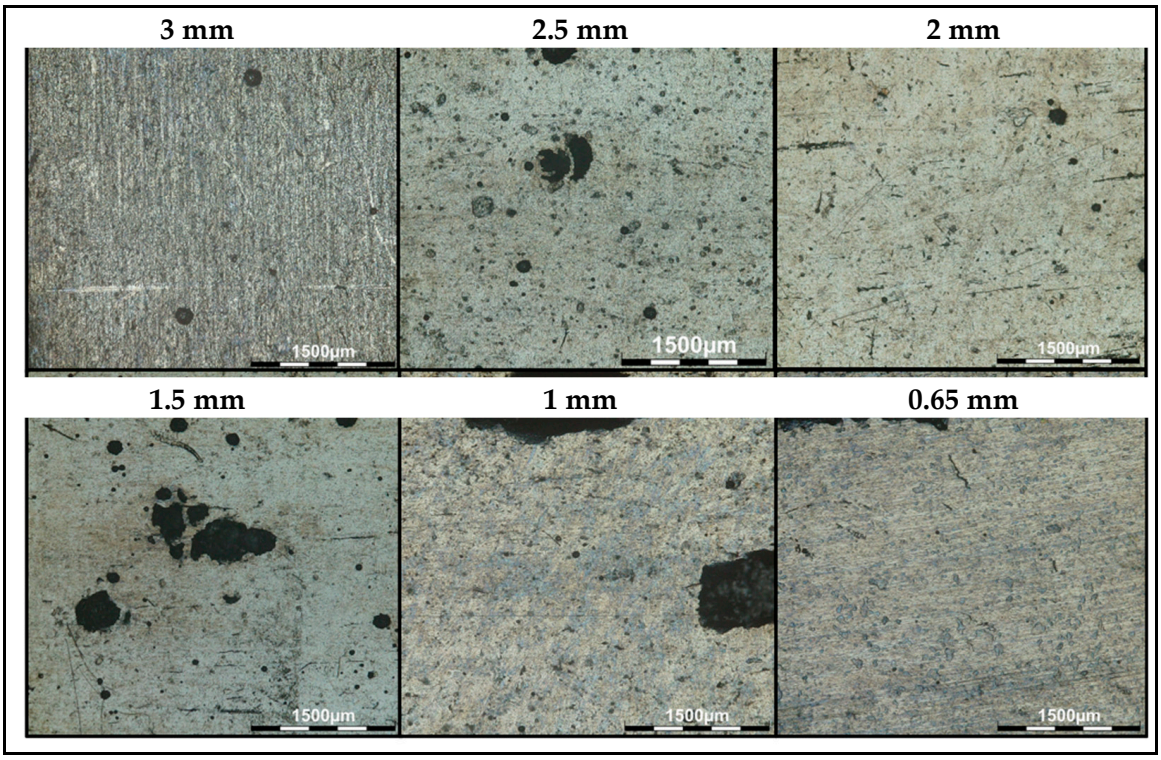


Figure 3. Macroscopic images of the surfaces of the test specimens.

In this case, weight loss of the test specimens provides a more reliable basis for comparing corrosion extent. Weight loss increased with increasing cold forming, indicating that specimens subjected to greater cold forming experienced greater corrosion-induced material loss. Macroscopic images are thus primarily useful for illustrating corrosion-induced surface changes, while weight loss provides a quantitative comparison of corrosion extent. Based on the microscopic images and weight loss, we conclude that complex corrosion occurred. The observed pitting corrosion does not account for the measured weight loss; therefore, other forms of corrosion likely occurred alongside pitting. Grain boundary and stress corrosion most likely occurred because of increased residual stress from the forming process and the appearance of the second phase (martensite).

Results on other grades and environments also indicate that deformation effects on pit nucleation and propagation must be distinguished from the net material loss recorded in a single immersion test [29,42].

3.4. Limitations of the Experiment

When evaluating the study results, several measurement uncertainties and experimental limitations must be considered. The surfaces of the test specimens exposed to corrosion were nearly identical; however, minor variations in geometric dimensions may have influenced the determined weight loss. Additional sources of uncertainty may have included the effects of removing corrosion products and cleaning the test specimens, as well as the accuracy of the weight measurements. The three test specimens examined in each material state represent a limited number of repetitions; therefore, a statistical evaluation of the results is only possible to a limited extent. Furthermore, the $FeCl_3$ solution test is primarily suitable for comparing different material states, and the results cannot be directly generalised to all natural or industrial corrosion environments. Based on the increase in weight loss, we can establish a correlation between forming and corrosion-induced material loss; however, further, more detailed investigations are needed to identify the corrosion

mechanism underlying this correlation unambiguously. Given the limited number of replicates, additional electrochemical measurements and quantitative image analysis would help test the proposed mechanistic interpretation [59].

3.5. Discussion of the Test Results

The most plausible explanation for the observed decrease in corrosion resistance is the microstructural heterogeneity introduced by cold rolling, particularly the development of deformation-induced martensite suggested by the optical micrographs. Differences in local electrochemical activity among the austenitic matrix, transformed regions, and deformation-affected areas may reduce passivation uniformity and promote preferential dissolution in the aggressive ferric chloride ($FeCl_3$) solution. This provides a possible link between increasing deformation and greater corrosion-induced weight loss. The present experiments establish an association between cold working, microstructural changes and corrosion weight loss; they do not isolate a single dominant mechanism. Accordingly, microstructural heterogeneity and its possible influence on local passivation constitute the leading mechanistic interpretation.

4. Conclusions

In this study, we investigated the corrosion behaviour of austenitic stainless steel 1.4301 (X5CrNi18-10/304) in various cold-rolled conditions. The austenite-martensite phase transformation microstructural changes are accompanied by hardening. The steel lost its uniform structure, and the corrosion resistance decreased. The corrosion test results revealed a clear trend between the degree of plastic deformation and corrosion-induced material loss.

Consistent with the literature, corrosion is complex, and corrosion resistance depends strongly on microstructure. The microstructure of austenitic 1.4301 steel can change with machining and environmental effects. The microscopy test results show the austenite-martensite phase transformation and the developed crystal structure. We did not test dislocation density, but based on the hardening of the test specimens, we suggest that dislocation density increases. We also infer that residual stress could increase in the microstructure, contributing to the increased corrosion weight loss. For industrial applications, understanding the corrosion behaviour of the widely used 1.4301 austenitic stainless steel is paramount.

Author Contributions: Conceptualisation, P.P. and Z.N.; methodology, T.A.K.; software, Z.N.; validation, P.P. and T.A.K.; formal analysis, Z.N.; investigation, P.P. and F.H.; resources, T.A.K. and F.H.; data curation, Z.N.; writing—original draft preparation, P.P.; writing—review and editing, T.A.K., P.P. and Z.N.; visualisation, P.P. and F.H.; supervision, T.A.K.; project administration, Z.N. All authors have read and agreed to the published version of the manuscript.

Funding: This research received no external funding.

Data Availability Statement: The original contributions presented in this study are included in the article. Further inquiries can be directed to the corresponding authors.

Conflicts of Interest: The authors declare no conflicts of interest.

References

1. Tiamiyu, A.A.; Eduok, U.; Szpunar, J.A.; Odeshi, A.G. Corrosion behavior of metastable AISI 321 austenitic stainless steel: Investigating the effect of grain size and prior plastic deformation on its degradation pattern in saline media. *Sci. Rep.* **2019**, *9*, 12116. [CrossRef] [PubMed]
2. Craig, B. Clarifying the Applicability of PREN Equations: A Short Focused Review. *Corrosion* **2021**, *77*, 382–385. [CrossRef] [PubMed]

3. Soccol, D. An updated Pitting Resistance Equivalent Number by proportional hazard survival models of reported pitting potentials. *Electrochim. Acta* **2024**, *511*, 145355. [CrossRef]
4. Sun, Y.; Tan, X.; Lan, R.; Ran, G.; Li, J.; Jiang, Y. Mechanisms of inclusion-induced pitting of stainless steels: A review. *J. Mater. Sci. Technol.* **2024**, *168*, 143–156. [CrossRef]
5. Jung, R.-H.; Tsuchiya, H.; Fujimoto, S. XPS characterisation of passive films formed on Type 304 stainless steel in humid atmosphere. *Corros. Sci.* **2012**, *58*, 62–68. [CrossRef]
6. Natarajan, R.; Palaniswamy, N.; Natesan, M.; Muralidharan, V.S. XPS Analysis of Passive Film on Stainless Steel. *Open Corros. J.* **2009**, *2*, 114–124. [CrossRef]
7. Nishimura, R.; Kudo, K. The effects of passive films formed on iron, nickel and austenitic stainless steels (SUS 304 and SUS 316) on pitting corrosion. *Corros. Sci.* **1990**, *31*, 479–484. [CrossRef]
8. Frankel, G.S. Pitting Corrosion of Metals: A Review of the Critical Factors. *J. Electrochem. Soc.* **1998**, *145*, 2186–2198. [CrossRef]
9. Shao, Z.; Yu, D.; Shao, D.; Du, Y.; Zheng, D.; Qiu, Z.; Wu, B. A protective role of Cl^- ion in corrosion of stainless steel. *Corros. Sci.* **2024**, *226*, 111631. [CrossRef]
10. Voisin, T.; Shi, R.; Zhu, Y.; Qi, Z.; Wu, M.; Sen-Britain, S.; Zhang, Y.; Qiu, S.R.; Wang, Y.M.; Thomas, S.; et al. Pitting Corrosion in 316L Stainless Steel Fabricated by Laser Powder Bed Fusion Additive Manufacturing: A Review and Perspective. *JOM* **2022**, *74*, 1668–1689. [CrossRef]
11. Stewart, J.; Williams, D.E. The initiation of pitting corrosion on austenitic stainless steel: On the role and importance of sulphide inclusions. *Corros. Sci.* **1992**, *33*, 457–474. [CrossRef]
12. Baker, M.A.; Castle, J.E. The initiation of pitting corrosion at MnS inclusions. *Corros. Sci.* **1993**, *34*, 667–682. [CrossRef]
13. Williams, D.E.; Kilburn, M.R.; Cliff, J.; Waterhouse, G.I.N. Composition changes around sulphide inclusions in stainless steels, and implications for the initiation of pitting corrosion. *Corros. Sci.* **2010**, *52*, 3702–3716. [CrossRef]
14. Jun, J.; Holguin, K.; Frankel, G.S. Pitting Corrosion of Very Clean Type 304 Stainless Steel. *Corrosion* **2014**, *70*, 146–155. [CrossRef] [PubMed]
15. Barbosa, M.; Scully, J.C. The role of repassivation kinetics in the measurement of the pitting potential of AISI 304 stainless steel by the scratch method. *Corros. Sci.* **1982**, *22*, 1025–1036. [CrossRef]
16. Chen, Y.; Tang, P.; Qiao, S.; Liu, S.; Yang, X.; Li, A. Dynamic breakdown of passive films on stainless steel during in situ thermal oxidation. *Corros. Sci.* **2022**, *209*, 110799. [CrossRef]
17. Ohnuki, Y.; Sato, S. In Situ Observation for Deformation-Induced Martensite Transformation (DIMT) during Tensile Deformation of 304 Stainless Steel Using Neutron Diffraction. Part I: Mechanical Response. *Quantum Beam Sci.* **2020**, *4*, 31. [CrossRef]
18. Zeuner, A.T.; Gerdt, L.; Ostwald, A.; Grün, P.; Barbosa, M.; Kaspar, J.; Zimmermann, M. Deformation-Induced Martensitic Transformation in Laser Cladded 304 Stainless Steel Coatings. *Materials* **2022**, *15*, 6392. [CrossRef] [PubMed]
19. Baker, M.A.; Castle, J.E. The initiation of pitting corrosion of stainless steels at oxide inclusions. *Corros. Sci.* **1992**, *33*, 1295–1312. [CrossRef]
20. Meng, Q.; Frankel, G.S.; Colijn, H.O.; Goss, S.H. Stainless-steel corrosion and MnS inclusions. *Nature* **2003**, *424*, 389–390. [CrossRef] [PubMed]
21. Zheng, J.; Hu, X.; Pan, C.; Fu, S.; Lin, P.; Chou, K. Effects of inclusions on the resistance to pitting corrosion of S32205 duplex stainless steel. *Mater. Corros.* **2018**, *69*, 572–579. [CrossRef]
22. Zhang, J.; Zhang, L.; Ren, Q.; Hu, J. Effect of Cerium on Mechanisms of Pitting Corrosion Induced by Inclusions in a 304 Stainless Steel. *ISIJ Int.* **2023**, *63*, 779–790. [CrossRef]
23. Park, J.H.; Kang, Y. Inclusions in Stainless Steels—A Review. *Steel Res. Int.* **2017**, *88*, 1700130. [CrossRef]
24. Kishore, K.; Chandan, A.K.; Sahoo, B.K.; Meena, L.K. Novel observation of dominant role of strain rate over strain during pre-straining on corrosion behaviour of 304L austenitic stainless steel. *Mater. Chem. Phys.* **2022**, *277*, 125522. [CrossRef]
25. *ASTM G48-25*; Standard Test Methods for Pitting and Crevice Corrosion Resistance of Stainless Steels and Related Alloys by Use of Ferric Chloride Solution. ASTM International: West Conshohocken, PA, USA, 2025. [CrossRef]
26. *ASTM G1-25*; Standard Practice for Preparing, Cleaning, and Evaluating Corrosion Test Specimens. ASTM International: West Conshohocken, PA, USA, 2025. [CrossRef]
27. Ahmad Buhairi, M.; Tóth, L.; Kovács, T.A. Review of Corrosion Test of Biomedical Titanium Alloys. In *Water as a Cardinal Area of Critical Infrastructure Protection*; Kovács, T.A., Stadler, R.G., Daruka, N., Eds.; Advanced Sciences and Technologies for Security Applications; Springer: Cham, Switzerland, 2026; pp. 15–25. [CrossRef]
28. Ohnuki, Y.; Sato, S. In Situ Observation for Deformation-Induced Martensite Transformation during Tensile Deformation of SUS 304 Stainless Steel by Using Neutron Diffraction. Part II: Transformation and Texture Formation Mechanisms. *Quantum Beam Sci.* **2021**, *5*, 6. [CrossRef]
29. Pradhan, S.K.; Bhuyan, P.; Bairi, L.R.; Mandal, S. Comprehending the role of individual microstructural features on electrochemical response and passive film behaviour in type 304 austenitic stainless steel. *Corros. Sci.* **2021**, *180*, 109187. [CrossRef]

30. Zhu, L.; Dong, Z.; Cai, G.; Li, Y.; Cui, Z. The effect of cold deformation on crevice corrosion and stress corrosion cracking behavior of 304 stainless steel. *Eng. Fail. Anal.* **2026**, *186*, 110515. [CrossRef]
31. Liu, M.; Huang, S.; Liu, Z.; Du, C. Investigations on the passive and pitting behaviors of the multiphase stainless steel in chlorine atmosphere. *J. Mater. Res. Technol.* **2024**, *28*, 3365–3375. [CrossRef]
32. Kamachi Mudali, U.; Shankar, P.; Ningshen, S.; Dayal, R.K.; Khatak, H.S.; Raj, B. On the pitting corrosion resistance of nitrogen alloyed cold worked austenitic stainless steels. *Corros. Sci.* **2002**, *44*, 2183–2198. [CrossRef]
33. Silva, P.M.O.; Filho, M.C.C.; da Cruz, J.A.; Sales, A.J.M. Influence on Pitting Corrosion Resistance of AISI 301LN and 316L Stainless Steels Subjected to Cold-Induced Deformation. *Metals* **2023**, *13*, 443. [CrossRef]
34. Das, A.; Roychowdhury, S.; Kain, V. Establishing the passive film stability formed at different depths from the surface of machined type 304L SS. *Corros. Sci.* **2020**, *176*, 109022. [CrossRef]
35. Salahi, S.; Kazemipour, M.; Nasiri, A. Effects of microstructural evolution on the corrosion properties of AISI 420 martensitic stainless steel during cold rolling process. *Mater. Chem. Phys.* **2021**, *263*, 123916. [CrossRef]
36. Peguet, L.; Malki, B.; Baroux, B. Influence of cold working on the pitting corrosion resistance of stainless steels. *Corros. Sci.* **2007**, *49*, 1933–1948. [CrossRef]
37. Monrrabal, G.; Bautista, A.; Guzmán, S.; Gutierrez, C.; Velasco, F. Influence of the cold working induced martensite on the electrochemical behavior of AISI 304 stainless steel surfaces. *J. Mater. Res. Technol.* **2019**, *8*, 1335–1346. [CrossRef]
38. Bachani, M.; Hayoune, A.; Fajoui, J.; Dubos, P.-A. Directional Corrosion Behavior of Cold-Rolled and Annealed 304L Stainless Steel: Role of Residual Stress and Phase Transformation. *Steel Res. Int.* **2025**, *96*, 285–294. [CrossRef]
39. Xu, Y.T.; Zhang, B.; Wei, X.X.; Wu, B.; Wang, Y.J.; Ma, X.L. Improving pitting resistance of Mo-containing stainless steels via chloride-assisted stabilisation of the passive film. *Corros. Sci.* **2024**, *227*, 111787. [CrossRef]
40. Choudhary, S.; Kelly, R.G.; Birbilis, N. On the origin of passive film breakdown and metastable pitting for stainless steel 316L. *Corros. Sci.* **2024**, *230*, 111911. [CrossRef]
41. Eguchi, K. Quantitative analysis of initiation site of pitting corrosion on type 304 austenitic stainless steel. *Corros. Sci.* **2023**, *221*, 111312. [CrossRef]
42. Sunada, S.; Maesato, H.; Yokoi, Y.; Notoya, H.; Sanuki, S.; Arai, K. Effect of Deformation-Induced Martensite on Pitting Corrosion of SUS304 Stainless Steel in H_2SO_4-NaCl Solution. *J. Jpn. Inst. Met.* **1990**, *54*, 1078–1086. [CrossRef]
43. Hahin, C.; Stoss, R.M.; Nelson, B.H.; Reucroft, P.J. Effect of Cold Work on the Corrosion Resistance of Nonsensitised Austenitic Stainless Steels in Nitric Acid. *Corrosion* **1976**, *32*, 229–238. [CrossRef]
44. Lv, J.; Luo, H. Effects of strain and strain-induced α′-martensite on passive films in AISI 304 austenitic stainless steel. *Mater. Sci. Eng. C* **2014**, *34*, 484–490. [CrossRef] [PubMed]
45. Milad, M.; Zreiba, N.; Elhalouani, F.; Baradai, C. The effect of cold work on structure and properties of AISI 304 stainless steel. *J. Mater. Process. Technol.* **2008**, *203*, 80–85. [CrossRef]
46. Truschner, M.; Janda, A.; Bodner, S.C.; Keplinger, A.; Mori, G. Effect of cold deformation on the stress corrosion cracking resistance of a high-strength stainless steel. *J. Mater. Sci.* **2022**, *57*, 20447–20461. [CrossRef]
47. Bensatte, O.; Garchani, F.E.E.; Kabiri, M.R. The influence of microstructure on the stress corrosion resistance of SS 304L. *J. Mater. Sci. Mater. Eng.* **2026**, *21*, 69. [CrossRef]
48. Dutta, A.; Tsai, M.H.; Nene, S.S. Microstructural complexity induced corrosion resistance in a novel compositionally complex alloy. *Mater. Chem. Phys.* **2025**, *333*, 130369. [CrossRef]
49. Gupta, K.K.; Yazdi, R.; Styrk-Geisler, M.; Mishin, O.V.; Ambat, R. Effect of Microstructure of Low-Alloy Steel on Corrosion Propagation in a Simulated CO_2 Environment 2022. *J. Electrochem. Soc. Vol.* **2022**, *169*, 11. [CrossRef]
50. Tyrała, D.; Pawłowski, B. Microstructural Aspects of Premature Pitting Corrosion of Steel Pipe–Case Study. *J. Fail. Anal. Prev.* **2022**, *22*, 2147–2153. [CrossRef]
51. Williamson, G.K.; Smallman, R.E., III. Dislocation densities in some annealed and cold-worked metals from measurements on the X-ray debye-scherrer spectrum. *Philos. Mag. A J. Theor. Exp. Appl. Phys.* **1956**, *1*, 34–46. [CrossRef]
52. Ishikawa, T. 1—Understanding and controlling microstructural evolution in metal forming: An overview. In *Woodhead Publishing Series in Metals and Surface Engineering, Microstructure Evolution in Metal Forming Processes*; Lin, J., Balint, D., Pietrzyk, M., Eds.; Woodhead Publishing: Cambridge, UK, 2012. [CrossRef]
53. Ghosh, S.; Rana, V.P.S.; Kain, V.; Mittal, V.; Baveja, S.K. Role of residual stresses induced by industrial fabrication on stress corrosion cracking susceptibility of austenitic stainless steel. *Mater. Des.* **2011**, *32*, 7. [CrossRef]
54. Smetana, M.; Gombarska, D.; Slezak, M.; Janousek, L.; Palcek, P. Investigation of the Mechanical and Magnetic Property Changes in Austenitic Stainless Steel AISI 304 After Cold Rolling Under Various Heat Treatment Conditions. *Appl. Sci.* **2025**, *15*, 2810. [CrossRef]
55. Cárcel-Carrasco, F.-J.; Pascual-Guillamón, M.; Solano García, L.; Salas Vicente, F.; Pérez-Puig, M.-A. Pitting Corrosion in AISI 304 Rolled Stainless Steel Welding at Different Deformation Levels. *Appl. Sci.* **2019**, *9*, 3265. [CrossRef]

56. Wang, J.; Zhang, L.F. Effects of cold deformation on electrochemical corrosion behaviors of 304 stainless steel. *Anti-Corros. Methods Mater.* **2017**, *64*, 252–262. [CrossRef]
57. Mohammadi, F.; Luo, J. Effect of cold work on erosion–corrosion of 304 stainless steel. *Corros. Sci.* **2011**, *53*, 549–556. [CrossRef]
58. Xu, C.; Hu, G. Effect of deformation-induced martensite on the pit propagation behavior of 304 stainless steel. *Anti-Corros. Methods Mater.* **2004**, *51*, 381–388. [CrossRef]
59. Eguchi, K. Predictive Modelling of Pitting Corrosion in Stainless Steel Using a NonStationary Poisson Process and a Diffusion-Controlled Growth Mechanism. *J. Electrochem. Soc.* **2026**, *173*, 111502. [CrossRef]

Disclaimer/Publisher's Note: The statements, opinions and data contained in all publications are solely those of the individual author(s) and contributor(s) and not of MDPI and/or the editor(s). MDPI and/or the editor(s) disclaim responsibility for any injury to people or property resulting from any ideas, methods, instructions or products referred to in the content.